The homogeneity scale and the growth rate of cosmic structures

Felipe Avila,[1]★ Armando Bernui,[1] Rafael C. Nunes,[2] Edilson de Carvalho[3] and Camila P. Novaes [2]

[1]*Observatório Nacional, Rua General José Cristino 77, São Cristóvão, 20921-400 Rio de Janeiro, RJ, Brazil*
[2]*Instituto Nacional de Pesquisas Espaciais, Av. dos Astronautas 1758, Jardim da Granja, São José dos Campos, SP, Brazil*
[3]*Centro de Estudos Superiores de Tabatinga, Universidade do Estado do Amazonas, 69640-000, Tabatinga, AM, Brazil*

ABSTRACT

We propose a novel approach to obtain the growth rate of cosmic structures, $f(z)$, from the evolution of the cosmic homogeneity scale, $R_H(z)$. Our methodology needs two ingredients in a specific functional form: $R_H(z)$ data and the matter two-point correlation function today, i.e. $\xi(r, z = 0)$. We use a Gaussian Process approach to reconstruct the function R_H. In the absence of suitable observational information of the matter correlation function in the local Universe, $z \simeq 0$, we assume a fiducial cosmology to obtain $\xi(r, z = 0)$. For this reason, our final result turns out to be a consistency test of the cosmological model assumed. Our results show a good agreement between: (i) the growth rate $f^{R_H}(z)$ obtained through our approach, (ii) the $f^{\Lambda CDM}(z)$ expected in the fiducial model, and (iii) the best-fitting $f(z)$ from data compiled in the literature. Moreover, using this data compilation, we perform a Gaussian Process to reconstruct the growth rate function $f^{data}(z)$ and compare it with the function $f^{R_H}(z)$ finding a concordance of $< 2\sigma$, a good result considering the few data available for both reconstruction processes. With more accurate $R_H(z)$ data, from forthcoming surveys, the homogeneity scale function might be better determined and would have the potential to discriminate between ΛCDM and alternative scenarios as a new cosmological observable.

Key words: Cosmology: Observations – Cosmology: Large-Scale Structure of the Universe.

1 INTRODUCTION

There is an increasing interest in measurements of the growth rate of cosmic structures, $f(z)$, because this function behaves differently for cosmological models based on different theories of gravity (see e.g. Huterer et al. 2015; Kazantzidis & Perivolaropoulos 2018; Basilakos & Anagnostopoulos 2020; Linder 2020; Velasquez-Toribio & Fabris 2020); notoriously, the concordance cosmological model Lambda cold dark matter (ΛCDM) is based on the theory of general relativity. In this scenario, precise measurements of $f(z)$ from diverse cosmological tracers measured at several redshifts would determine if the ΛCDM model correctly describes the evolution of the function $f(z)$ (Pezzotta et al. 2017; Aubert et al. 2020; Bautista et al. 2021; Avila et al. 2021), and to investigate classes of models based on modified gravity theory (Alam et al. 2020; Ntelis et al. 2020). But the interest in $f(z)$ is more fundamental. In fact, since the early works of Peebles (1965), Silk (1968), and Sunyaev & Zeldovich (1970), the theory of cosmological perturbations searches to describe the clustering evolution of the primordial density fluctuations, from the earliest times to the currently observed universe, where the growth rate of structures $f(z)$ represents a measurement of such clustering evolution.

The measurements of $f(z)$ can be done with good precision using the Redshift Space Distortions (RSD) approach, that is, studying the peculiar velocities caused by local gravitational potentials that introduce distortions in the two-point correlation function (2PCF; Kaiser 1987). Calculating the 2PCF from a galaxy survey, more precisely, the anisotropic correlation function, $\xi(s, \mu)$ (Hamilton 1992; Hamilton & Culhane 1995), one can constrain the product $f\sigma_8$, where σ_8 is the variance of the matter fluctuations at the scale of 8 Mpc/h (Juszkiewicz et al. 2009; Song & Percival 2009). For $f\sigma_8$ data compilations, see e.g. Zhang & Li (2018), Sagredo, Nesseris & Sapone (2018), and Alam et al. (2021).

The growth rate of cosmic structures, f, is defined as (Strauss & Willick 1995)

$$f(a) \equiv \frac{d \ln D(a)}{d \ln a},$$

where $D = D(a)$ is the linear growth function, and a is the scale factor in the Robertson–Walker metric, based on general relativity theory. Apply the above equation to a catalogue of cosmic objects to measure f does not work, because what one can measure directly from the data survey is the density contrast $\delta(r, a)$ and not the growth function $D(a)$. In this work, we propose a solution for this problem: search for a cosmic observable function that depends only on cosmic time (equivalently, on the redshift z or the scale factor a) instead of $D(a)$ in the above equation, being able to quantify the clustering evolution to provide a measurement of the growth rate of cosmic structures.

The Cosmological Principle is a fundamental piece in the concordance model of cosmology (Peebles 1980). It claims that, at sufficiently large scales, the universe is statistically homogeneous and isotropic (regarding the statistical isotropy of the universe, see

★ E-mail: felipeavila@on.br

e.g. Bernui et al. 2007; Bernui, Oliveira & Pereira 2014; Pereira & Pitrou 2015; Bengaly et al. 2017; Tarnopolski 2017; Dainotti, Del Vecchio & Tarnopolski 2018; Marques et al. 2018; Řípa & Shafieloo 2019). Several teams analysed galaxy surveys to calculate the scale where the transition from an inhomogeneous to a homogeneous distribution occurs, termed the homogeneity scale R_H (Scrimgeour et al. 2012; Laurent et al. 2016; Ntelis et al. 2017). For recent analyses, see e.g. Ntelis et al. (2019), Heinesen (2020), Pandey (2021a), Pandey & Sarkar (2021b), Gonçalves et al. (2021), De Marzo, Labini & Pietronero (2021), and Camacho & Gaztañaga (2021). In addition, analyses of the angular scale homogeneity have also been done to find the angular scale of homogenenity, θ_H, (Alonso et al. 2015; Gonçalves et al. 2018a; Avila et al. 2018, 2019), considered model independent measurements because one does not assume a cosmological model, as in the analyses of R_H, when one uses a fiducial cosmology to calculate 3D distances. At present, diverse deep astronomical surveys map large volumes of the universe, permitting to probe the evolution of R_H, although it is not as accurate as desirable. The next generation of surveys foresees a large number of R_H measurements with an improved accuracy (Amendola et al. 2018; Ivezić et al. 2019).

In this work, we will show that it is possible to use information from R_H, more precisely from the homogeneity scale evolution dR_H/dz, to obtain the cosmic evolution of the growth rate of structures $f(z)$. From the theoretical point of view, the homogeneity scale can be related to the 2PCF, $\xi(r)$ (Peebles 1980; Ntelis et al. 2017). From the linear perturbation theory, the redshift evolution of $\xi(r)$ is proportional to $D(z)^2$ then, $F[R_H(z)]D(z)^2 \propto$ cte, where F is a functional of the homogeneity scale function $R_H(z)$. As we shall see, this proportionality leads to the growth rate $f(z)$ through the redshift derivative of $\bar{\bar{\xi}}(R_H(z))$, the volume-averaged 2PCF. The approach to know the functional F needs to assume parameters that we determine assuming a ΛCDM fiducial cosmology. In this sense, our analyses should be considered as a test of consistency for the ΛCDM model.

The relationship between f and R_H indicates that with precise homogeneity scale data, $R_H(z)$, measured at several redshifts, one can determine with good accuracy the growth rate of cosmic structures $f = f(z)$, which in turn can be used to discriminate between the concordance ΛCDM and competing models based on modified gravity theories. Additionally, these data could be used in statistical analyses to find cosmological parameters. In other words, the homogeneity scale data, $R_H(z)$, would indeed play the role of a novel cosmological observable, as first discussed by Ntelis et al. (2019).

This work is organized as follows. In Section 2, we review the main equations of the linear theory of matter perturbations. In Section 3, we explain the methodology to obtain the transition scale to homogeneity and, for the first time, the relation between $R_H(z)$ and $f(z)$. In Section 4, we explain the reconstruction procedure to obtain a smooth curve of $R_H(z)$, and $dR_H(z)/dz$, both used then to obtain $f(z)$ according to our procedure. In Sections 5, we show our results and discuss them, while in Section 6, we present our conclusions.

2 GROWTH RATE OF COSMIC STRUCTURES

To describe the structure formation in an isotropic and homogeneous universe we used a perturbation approach: small deviation in the early universe has a slow evolution that can be described by a linear perturbation theory (Mukhanov, Feldman & Brandenberger 1992). One defines the density contrast as

$$\delta(\boldsymbol{r}, t) \equiv \frac{\rho(\boldsymbol{r}, t) - \bar{\rho}(t)}{\bar{\rho}(t)}, \tag{1}$$

where $\rho(\boldsymbol{r}, t)$ is the matter density at the comoving vector position $\boldsymbol{r}$ at cosmic time t and $\bar{\rho}(t)$ is the average matter density measured in the hyper-surface of constant t. In the linear and Newtonian regime, the gravitational potentials are small and the perturbation scale is smaller than the Hubble radius, $\lambda \ll c/H_0$, where c is the speed of light and H_0 is the Hubble constant. Over this condition, the structure formation is described with the fluid equations

$$\dot{\delta} = -\frac{1}{a}\nabla \cdot \boldsymbol{v}, \tag{2}$$

$$\dot{\boldsymbol{v}} + H\boldsymbol{v} = -\frac{1}{a\bar{\rho}}\nabla\delta p - \frac{1}{a}\nabla\delta\Phi, \tag{3}$$

$$\nabla^2\delta\Phi = 4\pi Ga^2\bar{\rho}\,\delta, \tag{4}$$

which are the continuity, Euler, and Poisson equations, respectively, perturbed at first order in comoving space. The dot corresponds to a partial derivative in cosmic time. The physical quantities $\boldsymbol{v}$, δp, and $\delta\Phi$ are the peculiar velocity, pressure, and the perturbed gravitational potential, respectively.

Combining equations (2), (3), and (4), and assuming adiabatic perturbations condition, we obtain the well known equation that describes the linear density contrast evolution of the matter density

$$\ddot{\delta}_m + 2\frac{\dot{a}}{a}\delta_m - 4\pi G\bar{\rho}_m\delta_m = 0. \tag{5}$$

In the linear approximation, the density contrast is a function of time only, that is, $\delta_m \sim D(t)$. From this, one can define the growth rate of cosmic structures as

$$f(a) \equiv \frac{a}{D}\frac{dD}{da} = \frac{d\ln D}{d\ln a}. \tag{6}$$

In the ΛCDM model we have the following approximation (Lahav et al. 1991)

$$f(z) \simeq \Omega_m^{0.6}(z) + \frac{\Omega_\Lambda}{70}\left(1 + \frac{1}{2}\Omega_m(z)\right), \tag{7}$$

where Ω_m and Ω_Λ are the matter and dark energy cosmological parameters, respectively. An alternative approximation is given by (Linder 2005; Linder & Cahn 2007)

$$f(z) = \Omega_m^\gamma(z), \tag{8}$$

where γ is the growth index. In the ΛCDM model, $\gamma = 6/11 \simeq 0.55$. This parameter assumes distinct values beyond ΛCDM cosmology (Basilakos 2012).

3 TRANSITION SCALE TO HOMOGENEITY

The most used methodology to study the homogeneity of galaxy or quasars distributions is to count the number of cosmic objects, N_{gal}, inside a sphere of radius r, and divide for N_{rand}, the equivalent count but for a random distribution, that has the same features as the original one. Then, we can define the *scaled counts-in-spheres*, $\mathcal{N}(< r)$ (Scrimgeour et al. 2012)

$$\mathcal{N}(< r) \equiv \frac{N_{gal}(< r)}{N_{rand}(< r)}, \tag{9}$$

where for a homogeneous distribution, at large scales, it goes to 1. It can be shown that $\mathcal{N}(< r)$ is related to the two-point correlation

function $\xi(r)$[1]

$$\mathcal{N}(<r) = 1 + \frac{3}{r^3}\int_0^r \xi(s)s^2\mathrm{d}s\,. \tag{10}$$

From the function $\mathcal{N}(<r)$, one can define the correlation dimension function $\mathcal{D}_2(r)$ (for details, see the appendix A in Ntelis et al. 2017),

$$\mathcal{D}_2(r) \equiv \frac{\mathrm{d}\ln\mathcal{N}(<r)}{rmd\,\ln r} + 3\,. \tag{11}$$

Despite the fact that most studies present both estimators, $\mathcal{N}(<r)$ and $\mathcal{D}_2(r)$, the result from the correlation dimension is considered more robust, because it is less correlated for most scales (Scrimgeour et al. 2012; Ntelis et al. 2017).

To finish this section, we discuss the arbitrary criterion used to determine the scale where the transition to homogeneity occurs, R_H. Consider the following equation

$$\mathcal{D}_2(R_H) = 3(1 - \epsilon)\,. \tag{12}$$

In an ideal situation, one expects $\epsilon = 0$, that is, when the homogeneity scale is attained the value of ϵ should be $\epsilon = 0$, such that the transition to homogeneity occurs on the scale at which $\mathcal{D}_2$ calculated from data achieve the value 3. However, due to systematic effects present in the galaxy surveys, Scrimgeour et al. (2012) suggested to fix the value of ϵ at, for example, 0.01, which gives us $\mathcal{D}_2(R_H) = 2.97$, that is, 1 per cent below 3. We assume this value because it is commonly adopted in the literature, and allow us to study the scale of homogeneity for different tracers in a large range of redshift. Anyhow, as we will show next, our methodology is independent of ϵ, due to the redshift derivative.

3.1 The growth rate of cosmic structures from the homogeneity scale

As mentioned above, the scaled counts-in-spheres, $\mathcal{N}(<r)$, is related to the two-point correlation function, $\xi(r;z)$, at redshift z

$$\xi(r=|\mathbf{x}-\mathbf{y}|;z) = \langle\delta(\mathbf{x};z)\delta(\mathbf{y};z)\rangle\,, \tag{13}$$

that is, is the spatial average of the product of the density contrasts evaluated at the arbitrary positions of a pair of galaxies, $\mathbf{x}$, $\mathbf{y}$, at redshift z. The redshift evolution of ξ can be obtained assuming for the equation (5) the solution $\delta(r;z) = \delta(r;z=0)D(z)$ (Schneider 2006). This leads to

$$\begin{aligned}\xi(r=|\mathbf{x}-\mathbf{y}|;z) &= \langle\delta(\mathbf{x};z)\delta(\mathbf{y};z)\rangle\\ &= D^2(z)\langle\delta(\mathbf{x};z=0)\delta(\mathbf{y};z=0)\rangle\\ &= D^2(z)\xi(r;z=0)\,,\end{aligned} \tag{14}$$

where $\xi(r;z=0)$ is the two-point correlation function at $z=0$. From equation (14), one can rewrite the scaled counts-in-spheres as

$$\mathcal{N}(<r,z) = 1 + D^2(z)\bar{\xi}(r)\,, \tag{15}$$

where

$$\bar{\xi}(r) \equiv \frac{3}{r^3}\int_0^r \xi(s,z=0)s^2\mathrm{d}s \tag{16}$$

is the volume average of the correlation function. From the equation (11), one has

$$\mathcal{D}_2(r,z) = \frac{rD^2(z)}{1+D^2(z)\bar{\xi}(r)}\frac{\mathrm{d}\bar{\xi}(r)}{\mathrm{d}r} + 3\,. \tag{17}$$

[1] For applications of the two-point correlation function in clustering analyses, see e.g. de Carvalho et al. (2018, 2021) and Carvalho et al. (2020).

It is useful to define the following quantity:

$$\zeta(r) \equiv \frac{\mathrm{d}\bar{\xi}(r)}{\mathrm{d}r}\,. \tag{18}$$

For the scale where the transition to homogeneity occurs, $r = R_H$, equation (17) becomes

$$R_H(z)D^2(z)\zeta[R_H(z)] = -3\epsilon\,(1 + D^2(z)\bar{\xi}[R_H(z)]) \simeq -3\epsilon\,, \tag{19}$$

where we consider only the first-order term. Now, taking the redshift derivative of equation (19) we have

$$\frac{\mathrm{d}}{\mathrm{d}z}\left(R_H D^2 \zeta\right) = 0\,. \tag{20}$$

This differential equation relates in a simple way $R_H(z)$ and $D(z)$.

Finally, separating each term of equation (20), we have

$$-\frac{2}{D}\frac{\mathrm{d}D}{\mathrm{d}z} = \frac{1}{R_H}\frac{\mathrm{d}R_H}{\mathrm{d}z} + \frac{1}{\zeta}\frac{\mathrm{d}\zeta}{\mathrm{d}z}\,. \tag{21}$$

Using the equation (6) in equation (21), we have

$$f(z) = \frac{1+z}{2}\left(\frac{1}{R_H}\frac{\mathrm{d}R_H}{\mathrm{d}z} + \frac{1}{\zeta}\frac{\mathrm{d}\zeta}{\mathrm{d}z}\right)\,, \tag{22}$$

which, explicitly, is independent of ϵ. To obtain $f(z)$, in addition to R_H data, we must obtain $\zeta[R_H(z)]$ from a correlation function in $z = 0$. Or, in a model dependent way, use an approximation, as we will describe in the next section.

4 TESTING THE MODEL

In this section, we describe our methodology, aimed to solve equation (22), and apply it to a set of R_H data to obtain the growth function $f(z)$. First, we present the data, and secondly, we detail the approximation used to define $\zeta(R_H)$. By last, we describe the Gaussian Process methodology used to reconstruct R_H and $\mathrm{d}R_H/\mathrm{d}z$.

4.1 Data

Here, we use two sets of R_H measurements. The first one is provided by Ntelis et al. (2017), through the study of the CMASS galaxy sample of the BOSS survey, they calculated the transition to homogeneity for 5 uncorrelated redshift bins in the interval $0.43-0.70$. The authors analysed separately the North (NGC) and South Galactic Caps (SGC), at the same redshift bins, obtaining five independent measurements for each of them (i.e. a total of 10 R_H data). The second R_H data set comes from Gonçalves et al. (2018b), who analysed the quasars sample from the fourteenth data release of the Sloan Digital Sky Survey (SDSS-IV DR14) in the redshift interval $0.80-2.24$. They measured R_H in each one of four uncorrelated redshift bins (i.e. 4 R_H data) studied employing two estimators to calculate $\mathcal{N}(<r)$: Landy-Szalay (LS) and Peebles–Hauser (PH) estimators, obtaining similar results in both cases. In Table 1, we list these $R_H(z)$ data with their respective redshifts.

Following Ntelis et al. (2019), we combine the R_H data from NGC (j) and SGC (k) using a weighted average, defined as

$$R_H^w(z_i) \equiv \left(\frac{1}{\sigma_j^2(z_i)} + \frac{1}{\sigma_k^2(z_i)}\right)^{-1} \times \left(\frac{R_H^j(z_i)}{\sigma_j^2(z_i)} + \frac{R_H^k(z_i)}{\sigma_k^2(z_i)}\right)\,, \tag{23}$$

where σ_j, σ_k, and R_H^j, R_H^k are, respectively, the errors and data for two independent measurements, j and k, in the same redshift, z_i. At first order, we can neglect the covariance between redshift bins. For the Gonçalves et al. (2018b) data, we choose the data from the PH estimator to optimize our analyses.
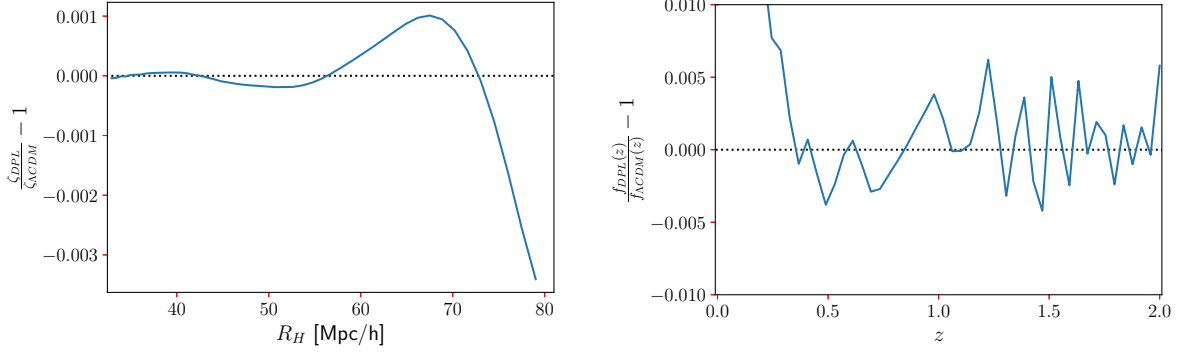
Figure 1. Left-hand panel: Relative error between $\zeta[R_H]$ as fitted using the DPL approximation (equation 24) and the expectation from the ΛCDM model. Right-hand panel: Relative error of the cosmic growth rate $f(z)$ calculated using equation (26) with respect to $f(z)$ obtained using the equation (6) assuming the same ΛCDM fiducial cosmology; one also observes the noisy pattern caused by the numerical derivative.

Notice that the R_H we use here are already corrected by the corresponding bias factor. The bias for each redshift bin have been determined by the respective authors, which provided the bias-corrected measurements. This is important because each homogeneity scale measurement is calculated for a specific tracer and a proper combination of these data requires their conversion to the corresponding transition scale for the underlying matter distribution.

4.2 Double power-law approximation for $\zeta(R_H)$

In order to use the selected R_H data sample to calculate $f^{R_H}(z) = f(z)$, using equation (22), we need to define $\zeta(R_H)$. For this we approximate $\zeta(R_H)$ by a Double Power Law (DPL) function, similar to that one used in the study of the AGN luminosity function (Kulkarni, Worseck & Hennawi [2019])

$$\zeta(R_H) = -\frac{C R_H^{-1}}{(R_H/R_\star)^\alpha + (R_H/R_\star)^\beta} \,, \tag{24}$$

where C, $R_\star$, α, and β are the parameters to be adjusted. Taking its redshift derivative

$$\frac{1}{\zeta}\frac{d\zeta}{dz} = -\frac{(1+\alpha)(R_H/R_\star)^\alpha + (1+\beta)(R_H/R_\star)^\beta}{(R_H/R_\star)^\alpha + (R_H/R_\star)^\beta}\frac{1}{R_H}\frac{dR_H}{dz} \,, \tag{25}$$

the growth rate can be written as

$$f^{R_H}(z) = \frac{1+z}{2}\left[1 - \frac{(1+\alpha)\left(\frac{R_H}{R_\star}\right)^\alpha + (1+\beta)\left(\frac{R_H}{R_\star}\right)^\beta}{\left(\frac{R_H}{R_\star}\right)^\alpha + \left(\frac{R_H}{R_\star}\right)^\beta}\right]\frac{1}{R_H}\frac{dR_H}{dz} \,, \tag{26}$$

where $R_H = R_H(z)$.

We fit the four free parameters of the DPL approximation to the theoretical expectation for $\zeta(R_H)$, for R_H corresponding the redshift range $0 < z < 2$, considering the ΛCDM model baseline obtained from Planck Collaboration ([2020]), that is, $h = 0.6727$, $\Omega_c h^2 = 0.1202$, $\Omega_b h^2 = 0.02236$, $\Sigma m_\nu = 0.0600$, $n_s = 0.9649$, $\sigma_8 = 0.8120$, and $\ln(10^{10} A_s) = 3.045$. For this we employ the public code `cosmopit`[2] (Ntelis et al. [2017], [2018]) to produce $\zeta(R_H)^{\Lambda CDM}$, which uses the public code `CLASS`[3] (Lesgourgues [2011]; Blas, Lesgourgues & Tram [2011]) as a background. We obtain for these parameters $[R_\star, \alpha, \beta, C] = [46.16, 2.76, 1.12, 0.19]$, whose

---

[2]https://github.com/lontelis/cosmopit
[3]https://github.com/lesgourg/class_public

Table 1. The $R_H(z)$ data used in the analyses.

| z	R_H (Mpc h^{-1})		Reference
	NGC	SGC	
0.457	64.20 ± 1.30	66.70 ± 1.60	Ntelis et al. ([2017])
0.511	65.40 ± 0.90	63.90 ± 1.50	
0.565	62.60 ± 0.80	65.20 ± 1.60	
0.619	60.40 ± 0.80	60.10 ± 1.10	
0.673	59.00 ± 0.80	60.10 ± 1.80	
	PH	LS	
0.985	48.78 ± 3.82	52.93 ± 7.55	Gonçalves et al. ([2018b])
1.350	40.56 ± 3.39	40.43 ± 5.64	
1.690	36.19 ± 3.45	36.66 ± 4.80	
2.075	27.91 ± 3.91	29.94 ± 3.35	

error for each of them is less than 1 per cent. The plot on the left-hand panel of Fig. [1] shows the relative error between the input ΛCDM expectation and the fitted DPL approximation, where we observe a good agreement on all scales. The maximum discrepancy of 0.3 per cent appears at the largest R_H scales considered here. This occurs due to the effect introduced in $\zeta(R_H)$ by the presence of the BAO feature at $\sim 100 h^{-1}$Mpc in the correlation function, then the DPL approximation fails to model the large scales. See Appendix A for more details. Notice that, although the methodology does not depend on ϵ explicitly, as shown in equation (22), we follow Scrimgeour et al. ([2012]) and fix this value to $\epsilon = 0.01$ to obtain the $\zeta[R_H(z)]^{\Lambda CDM}$ function and then calculate the best-fitting parameters for the DPL approximation. In Appendix B, we test the criterion for ϵ and the dependence of our methodology on some cosmological parameters. Additionally, the right panel of Fig. [1] shows the relative error between the cosmic growth rate $f^{R_H}(z)$ calculated using the DPL approximation equation (26) and that obtained from equation (6) assuming the ΛCDM fiducial model. As observed, for almost the whole redshift interval, we observe a maximum deviation of ~ 0.5 per cent, again at low redshifts, where we also notice the noisy pattern caused by the numerical derivative. Note that, since we have a small set of R_H data, we use a reconstructed function from them to be able to appropriately calculate the derivative dR_H/dz in equation (26), a procedure detailed in the following section.

4.3 Gaussian process regression

To extract maximum cosmological information from the R_H data listed in Table [1] we perform a Gaussian Process (GP) Regression
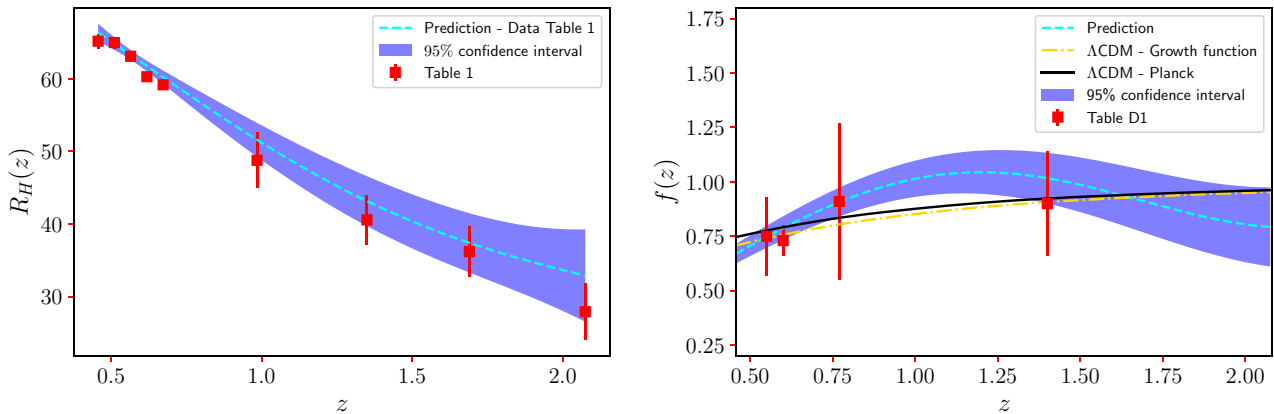
Figure 2. Left-hand panel: Reconstruction of the homogeneity scale function $R_{\rm H}(z)$ using Gaussian Process (dashed line) and the $R_{\rm H}$ measurements (red squares) presented in Table 1 (see the text for details about the data set); the shadow represents the 95 per cent CL. Right-hand panel: Derivation of the growth rate of structures $f^{R_{\rm H}}(z)$ (dashed line) using the reconstructed function $R_{\rm H}(z)$, shown in the left-hand panel plot, and the equation (26), where the shadow represents the 95 per cent CL. The solid line represents the expression expected in the ΛCDM model, $f^{\Lambda\rm CDM}(z)$, obtained from equation (6) with $\Omega_m^{\rm Planck} = 0.315$; instead, the dot–dashed line shows the expected growth rate using equation (6) but with $\Omega_m = 0.270^{+0.079}_{-0.073}$, a value obtained from the best-fitting analyses of the $f(z)$ data as shown in Fig. 4 (the red squares are the data listed in Table D1). Comparing the $f^{R_{\rm H}}(z)$ (dashed line) and the best-fitting $f(z)$ (dot–dashed line) functions we found an agreement of $<2\sigma$ (considering the corresponding uncertainties, not shown in the figure to avoid excess of information).

method, obtaining in this way a smooth curve for $R_{\rm H}(z)$ and, by numerical derivation, for $dR_{\rm H}/dz$; this information is then used in equation (26) to obtain the $f^{R_{\rm H}}(z)$ function. The GP consists of generic supervised learning method designed to solve regression and probabilistic classification problems, where we can interpolate the observations and compute empirical confidence intervals and a prediction in some region of interest (Rasmussen 2003; Pezzotta et al. 2017). The GP method design from machine learning techniques is the state of the art to obtain statistical information and model prediction from some previously known information or data. In the cosmological context, GP techniques has been used to reconstruct cosmological parameters, like the dark energy equation of state, $\omega(z)$, the expansion rate of the universe, the cosmic growth rate, and other cosmological functions (see e.g. Seikel, Clarkson & Smith 2012; Shafieloo, Kim & Linder 2012; Zhang & Li 2018; Marques et al. 2019; 2020; ; Nunes et al. 2020a; Nunes & Bernui 2020b; Renzi & Silvestri 2020; Bonilla, Kumar & Nunes 2021a; Bonilla et al. 2021b; Colgáin & Sheikh-Jabbari 2021; Escamilla-Rivera, Said & Mifsud 2021; Sun, Jiao & Zhang 2021 for a short list of references).

The main advantage in this procedure is that it is able to make a non-parametric inference using only a few physical considerations and minimal cosmological assumptions. Our aim is to reconstruct a function $F(x_i)$ from a set of its measured values $F(x_i) \pm \sigma_i$, where x_i represent our data sample. It assumes that the value of the function at any point x_i follows a Gaussian distribution. The value of the function at x_i is correlated with the value at other point x_i'. Thus, a GP is defined as

$$F(x_i) = \mathcal{GP}(\mu(x_i), {\rm cov}[F(x_i), F(x_i)]), \tag{27}$$

where $\mu(x_i)$ and ${\rm cov}[F(x_i), F(x_i)]$ are the mean and the variance of the variable at x_i, respectively. For the reconstruction of the function $F(x_i)$, the covariance between the values of this function at different positions x_i can be modeled as

$$\mathrm{cov}[F(x), F(x')] = k(x, x'), \tag{28}$$

where $k(x, x')$ is known as the kernel function. The kernel choice is often crucial for obtaining good results regarding the reconstruction of the function of interest.

The kernel most commonly used is the standard Gaussian Squared-Exponential approach, which is defined as

$$k\left(x, x'\right) = \sigma_F^2 \exp\left(-\frac{|x - x'|^2}{2l^2}\right), \tag{29}$$

where σ_F^2 is the signal variance, which controls the strength of the correlation of the function F, and l is the length scale that determines the capacity to model the main characteristics (global and local) in the evaluation region to be predicted (or coherence length of the correlation in x). These two parameters are often called hyperparameters.

It is well known that depending on the data set in analysis, the kernel choice is an important point. We verify that our data set is well modelled by the choice above, and that other kernels do not produce major changes in our main results (see Appendix B). In what follows, we discuss our results.

5 RESULTS AND DISCUSSIONS

In this section, we present our main results. We performed a GP to reconstruct the homogeneity scale, $R_H(z)$. From this, using the DPL model, we can obtain $f^{R_{\rm H}}(z)$. Also, we perform the GP to our $f(z)$ data compilation. Finally, we study the parameter space $H_0 - \Omega_m$ from the same data compilation.

5.1 Results of the reconstruction of $f^{R_{\rm H}}(z)$ and $f(z)$

In obtaining the results to be described in this section, we use the Scikit-learn code (Pedregosa et al. 2011), which is a PYTHON module integrating a wide range of state-of-the-art machine learning algorithms, to model the GP described in the previous section. The hyperparameters σ_F^2 and l are optimized during the fitting by maximizing the log-marginal-likelihood.

The left-hand panel of Fig. 2 shows the best-fitting prediction of the reconstruction GP of the homogeneity scale function $R_H(z)$, at 95 per cent CL, from the data sample listed in Table 1 (represented by red squares in this plot). As verified in this plot, the $R_H(z)$ data reveals the expected behaviour in the evolution of the matter clustering in
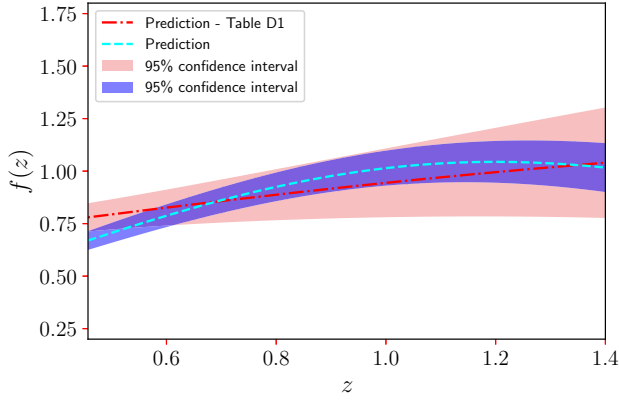
Figure 3. Comparison of the growth rate $f^{R_H}(z)$ obtained from equation (26) (dashed line) and the GP reconstructed function $f^{data}(z)$ (dot–dashed line) using the data compilation given in Table D1. Both reconstructed functions show a significant overlapping of the respective 2σ regions (shaded areas).
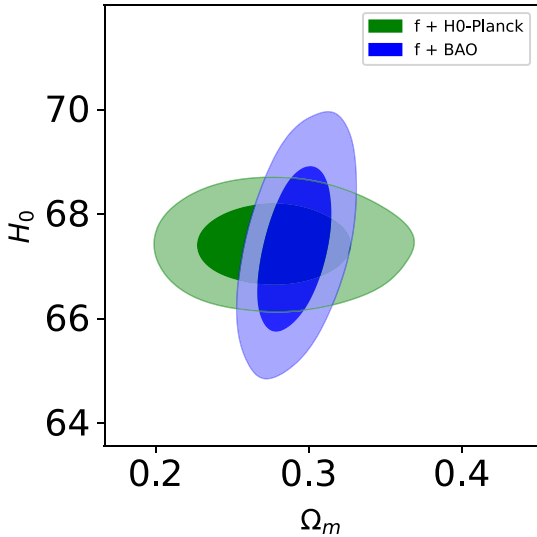
Figure 4. The 68 per cent (dark shaded area) and 95 per cent (light shaded area) CLs regions, respectively, on the parametric space $H_0 - \Omega_m$ from $f(z)$ + Planck-H_0 prior and $f(z)$ + BAO joint analyses. The parameter H_0 is measured in the units of km s^{-1} Mpc^{-1}.

the Universe, going from a nearly homogeneous situation at high redshift to a non-linear clustered matter at low redshift where the homogeneity scale is attained only at large scales.

We use these $R_H(z)$ data to obtain the evolution of the growth rate of cosmic structures, $f^{R_H}(z)$, according to equation (26) following the procedure described in Section 3.1. Our result can be observed on the right panel of Fig. 2, where $f^{R_H}(z)$ is plotted as a dashed line and the current measurements of $f(z)$, listed in the Table D1 in appendix D, as red squares. It is important to mention that f^{R_H} obtained through our procedure does not represent a direct $f(z)$ measurement, but a non-parametric inference that can describe the evolution of the growth rate function from minimal cosmological assumptions. We also show for comparison the ΛCDM expected growth rate using equation (6) in two cases: using $\Omega_m^{Planck} = 0.315$ (continuous line) from the Planck cosmological parameters, and using $\Omega_m = 0.26$ (dot–dashed line) from the best-fitting data analyses shown in Fig. 4.

On the other hand, it is interesting to compare the growth rate of cosmic structures $f^{R_H}(z)$ from the evolution of the cosmic homogeneity scale, with the $f^{data}(z)$ resulting from a GP reconstruction using the current $f(z)$ data listed in Table D1. Notice that, the reconstruction procedure of $f^{R_H}(z)$ is performed in the redshift interval with $R_H(z)$ data, namely $z \in [0.457, 2.075]$, while the reconstruction procedure of $f^{data}(z)$ is done with $f(z)$ data in the interval $z \in [0.013, 1.4]$. Then, for the comparative analysis we consider the common redshift interval: $z \in [0.457, 1.4]$ shown in Fig. 3, where we observe that both functions agree well ($<2\sigma$ level), overlapping significantly.

One should notice that a plausible systematic present in the R_H data, listed in Table 1, is sourced by the necessity to assume a fiducial cosmology to calculate the 3D distances to the cosmic objects (galaxies or quasars), so that one can determine the 3D separation distance between each pair of them, information used to measure R_H. As a matter of fact, the $R_H(z)$ measurements are model dependent and one should be cautious with this. For instance, the analyses done by Ntelis et al. (2017) assumed a fiducial cosmology different to that assumed by Gonçalves et al. (2018b), a fact that helps to explain why in the left panel of Fig. 2 one data set appear slightly over and the other slightly under the reconstructed function (dashed line).

5.2 Validation test of $H_0 - \Omega_m$ plane estimates from the current compilation of growth rate data

As a final discussion of this section, we will check what our compilation of $f(z)$ data, shown in Table D1, can tell us about the ΛCDM baseline. Let us perform an analysis in three steps:

(i) To constrain Ω_m we consider $f(z)$ data (see Table D1) only.

(ii) A combination $f(z)$ data plus a Gaussian prior on H_0 using the Planck-CMB best fit. Note that we are within a ΛCDM baseline, so to use Planck-CMB information in ΛCDM itself context is just to improve the constraint on Ω_m.

(iii) We consider the joint analysis $f(z)$ + BAO. In this work, we consider the most recent BAO data compilation comprised of the $D_V(z)/r_d$, $D_M(z)/r_d$, and $D_H(z)/r_d$ measurements compiled in Table 3 in Alam et al. (2021).

We use the Metropolis-Hastings mode in `CLASS` + `MontePython` code (Lesgourgues 2011; Blas et al. 2011; Audren et al. 2013; Brinckmann & Lesgourgues 2019) to derive the constraints on cosmological parameters from the data sets described above, ensuring a Gelman–Rubin convergence criterion of $R - 1 < 10^{-3}$.

Fig. 4 shows the parameter space in the $H_0 - \Omega_m$ plane at 68 per cent and 95 per cent CL from $f(z)$ + Planck-H_0 prior and $f(z)$ + BAO joint analyses, where $f(z)$ data refers to the measurements presented in Table D1. The summary of the main results of our statistical analyses at 68 per cent CL are: $\Omega_m = 0.27^{+0.079}_{-0.073}$ ($f(z)$ data only), $\Omega_m = 0.279^{+0.066}_{-0.067}$ ($f(z)$ + H_0-Planck) and $\Omega_m = 0.291^{+0.033}_{-0.030}$ and $H_0 = 67.4^{+2.1}_{-2.0}$ km s^{-1} Mpc^{-1} from $f(z)$ + BAO combination.

As well known, there is a growing tension for low z measurements of $f(z)$ and it is weaker than the Planck-ΛCDM predictions (see Di Valentino et al. 2021; Perivolaropoulos & Skara 2021 and reference therein for a review and the recent discussion presented in Nunes & Vagnozzi 2021). Our results here also confirm that growth rate data based on the measurements in Table D1 predict a suppression on the amplitude of the matter density perturbation at low z due the low Ω_m estimation in comparison with that from the Planck-ΛCDM, $\Omega_m = 0.315 \pm 0.007$ (Planck Collaboration 2020). On the right-hand panel of Fig. 2, we also show the theoretical curve assuming our constraint

on Ω_m. Despite predicting a low Ω_m best-fitting value in our analysis, the error bar estimates are in agreement with Planck CMB at $<1\sigma$.

6 CONCLUSIONS

Measurements of the growth rate of cosmic structures, f, have the potential to differentiate between the theory of general relativity, that supports the concordance model ΛCDM, from alternative scenarios based on modified gravity models. Besides the efforts, the current uncertainties in such measurements do not allow to discern between competing models of modified gravity.

This motivated us to search for a cosmological observable that depends only on the cosmic time t, or equivalently on the redshift z. We propose to use the transition scale to homogeneity, $R_{\rm H}(z)$, to know the evolution of the growth rate $f = f(z)$. As shown in the Section 3.1, the relation between $R_{\rm H}$ and f is not direct and one needs two ingredients: (i) a set of $\{R_{\rm H}(z_i)\}$ data – in the redshift interval of interest – to reconstruct the continuous function $R_{\rm H}(z)$ and to perform its redshift derivative; and (ii) the matter two-point correlation function at $z = 0$, $\xi(r, z = 0)$, that analyses distance scales of the order of the homogeneity scale. However, there is no observational data to construct $\xi(r, z = 0)$, and one has to assume a fiducial cosmology to obtain it. For this reason, our analyses and results are actually consistency tests of the cosmological model assumed.

Using GP, our reconstruction of the homogeneity scale function $R_{\rm H}(z)$ done in Section 5 shows the expected behaviour, although the current data set is small and with large errors (see Table 1). With the functions $R_{\rm H}(z)$ and $\xi(r, z = 0)$, and following our procedure, we use them in equation (26) to obtain the growth rate of cosmic structures $f^{R_{\rm H}}(z)$. Our results, displayed in the right-hand panel of fig. 2, show a good agreement between: (i) the growth rate $f^{R_{\rm H}}(z)$ obtained through our approach, (ii) the $f^{\Lambda\rm CDM}(z)$ expected in the fiducial model, and (iii) the best-fit $f(z)$ from the set of $\{f(z_i)\}$ measurements available in the literature. Moreover, using this compilation of $\{f(z_i)\}$ data (see Appendix D), we perform a GP to reconstruct the growth rate function $f^{\rm data}(z)$ and compare it with the function $f^{R_{\rm H}}(z)$ obtained from our approach, finding a concordance of $<2\sigma$ as observed in Fig. 3 (notice the significant overlapping of their 2σ regions). This is a good result considering the few data available for both reconstruction processes.

It is worth to note that our approach to find the growth rate of cosmic structures, $f(z)$, from the evolution of the cosmic homogeneity scale, $R_{\rm H}(z)$, relies on the definition of the homogeneity scale which is not unique (see e.g. Pandey 2021a; Pandey & Sarkar 2021b); in our approach, the homogeneity scale is provided by the estimator D_2 through the analyses of the universe fractal structure (Scrimgeour et al. 2012).

The relationship found between f and $R_{\rm H}$ indicates that with precise homogeneity scale data, $R_{\rm H}(z)$, measured at several redshifts from forthcoming surveys (see e.g. Amendola et al. 2018; Ivezić et al. 2019), one can determine with good accuracy the growth rate of cosmic structures $f = f(z)$, which in turn can be used to discriminate between the concordance ΛCDM and competing models based on modified gravity theories. Moreover, these data could be used in statistical analyses to find cosmological parameters. In summary, the homogeneity scale data, $R_{\rm H}(z)$, would indeed play the role of a novel cosmological observable, as first discussed by Ntelis et al. (2019).

DATA AVAILABILITY

The data underlying this article will be shared on request to the corresponding author.

REFERENCES

Alam S. et al., 2020, preprint (arXiv:2011.05771)
Alam S. et al., 2021, Phys. Rev. D, 103, 083533
Alonso D. et al., 2015, MNRAS, 449, 670
Amendola L. et al., 2018, Living Rev. Rel., 21, 2
Aubert M. et al., 2020, preprint (arXiv:2007.09013)
Audren B. et al., 2013, J. Cosmol. Astropart. Phys., 02, 001
Avila F. et al., 2018, J. Cosmol. Astropart. Phys., 12, 041
Avila F. et al., 2019, MNRAS, 488, 1481
Avila F. et al., 2021, MNRAS, 505, 3404
Basilakos S., 2012, Int. J. Mod. Phys. D, 21, 1250064
Basilakos S., Anagnostopoulos F. K., 2020, Eur. Phys. J. C, 80, 1
Bautista J. E. et al., 2021, MNRAS, 500, 736
Bengaly C. A. P., Bernui A., Ferreira I. S., Alcaniz J. S., 2017, MNRAS, 466, 2799
Bernui A., Mota B., Rebouças M. J., Tavakol R., 2007, Int. J. Mod. Phys. D, 16, 411
Bernui A., Oliveira A. F., Pereira T. S., 2014, J. Cosmol. Astropart. Phys., 10, 041
Blake C. et al., 2011, MNRAS, 415, 2876
Blake C. et al., 2013, MNRAS, 436, 3089
Blas D., Lesgourgues J., Tram T., 2011, J. Cosmol. Astropart. Phys., 07, 034
Bonilla A. et al., 2021, preprint (arXiv:2102.06149)
Bonilla A., Kumar S., Nunes R. C., 2021, Eur. Phys. J. C, 81, 1
Brinckmann T., Lesgourgues J., 2019, Phys. Dark Universe, 24, 100260
Camacho B., Gaztañaga E., 2021, preprint (arXiv:2106.14303)
Carvalho G. C. et al., 2020, Astropart. Phys., 119, 102432
Colgáin E. Ó., Sheikh-Jabbari M. M., 2021, preprint (arXiv:2101.08565)
Da Ângela J. et al., 2008, MNRAS, 383, 565
Dainotti M. G., Del Vecchio R., Tarnopolski M., 2018, Adv. Astron., 2018, 4969503
de Carvalho E. et al., 2018, J. Cosmol. Astropart. Phys., 04, 064
de Carvalho E. et al., 2021, A&A, 649, A20
De Marzo G., Labini F. S., Pietronero L., 2021, A&A, 651, A114
Di Valentino E. et al., 2021, Astropart. Phys., 131, 102604
Eisenstein D. J., Hu W., 1998, ApJ, 496, 605
Escamilla-Rivera C., Said J. L., Mifsud J., 2021, J. Cosmol. Astropart. Phys., 10, 016
Gonçalves R. S., 2021, J. Cosmol. Astropart. Phys., 03, 029
Gonçalves R. S. et al., 2018a, MNRAS, 475, L20
Gonçalves R. S. et al., 2018b, MNRAS, 481, 5270
Guzzo L., 2008, Nature, 451, 541
Hamilton A. J. S., 1992, ApJ, 385, L5
Hamilton A. J. S., Culhane M., 1995, MNRAS, 278, 73
Hawkins E. et al., 2003, MNRAS, 346, 78
Heinesen A., 2020, J. Cosmol. Astropart. Phys., 10, 052
Huterer D. et al., 2015, Astropart. Phys., 63, 23
Ivezić Ž. et al., 2019, ApJ, 873, 111
Juszkiewicz R. et al., 2009, J. Cosmol. Astropart. Phys., 2, 021
Kaiser N., 1987, MNRAS, 227, 1
Kazantzidis L., Perivolaropoulos L., 2018, Phys. Rev. D, 97, 103503
Kulkarni G., Worseck G., Hennawi J. F., 2019, MNRAS, 488, 1035
Lahav O. et al., 1991, MNRAS, 251, 128
Laurent P., 2016, J. Cosmol. Astropart. Phys., 11, 060
Lesgourgues J., 2011, preprint (arXiv:1104.2932)
Linder E. V., 2005, Phys. Rev. D, 72, 043529
Linder E. V., 2020, J. Cosmol. Astropart. Phys., 10, 042

Linder E. V., Cahn R. N., 2007, Astropart. Phys., 28, 481

Marques G. A., Novaes C. P., Bernui A., Ferreira I. S., 2018, MNRAS, 473, 165

Marques G. A. et al., 2019, J. Cosmol. Astropart. Phys., 06, 019

Marques G. A., Liu J., Huffenberger K. M., Colin Hill J., 2020, ApJ, 904, 182

Mukhanov V. F., Feldman H. A., Brandenberger R. H., 1992, Phys. Rep., 215, 203

Ntelis P. et al., 2017, J. Cosmol. Astropart. Phys., 06, 019

Ntelis P. et al., 2018, J. Cosmol. Astropart. Phys., 12, 014

Ntelis P. et al., 2019, preprint (arXiv:1904.06135)

Ntelis P. et al., 2020, preprint (arXiv:2010.06707)

Nunes R. C., Bernui A., 2020b, Eur. Phys. J. C, 80, 1025

Nunes R. C., Vagnozzi S., 2021, MNRAS, 505, 5427

Nunes R. C. et al., 2016, J. Cosmol. Astropart. Phys., 08, 051

Nunes R. C., Yadav S. K., Jesus J. F., Bernui A., 2020a, MNRAS, 497, 2133

Pandey B., 2021, J. Cosmol. Astropart. Phys., 02, 023

Pandey B., Sarkar S., 2021, J. Cosmol. Astropart. Phys., 07, 019

Pedregosa F. et al., 2011, J. Mach. Learn. Res., 12, 2825

Peebles P. J. E., 1965, ApJ, 142, 1317

Peebles P. J. E., 1980, The large-scale structure of the universe. Princeton Univ. Press, Princeton, NJ

Pereira T., Pitrou C., 2015, Comptes rendus - Physique, 16, 1027

Perivolaropoulos L., Skara F., 2021, preprint (arXiv:2105.05208)

Pezzotta A. et al., 2017, A&A, 604, A33

Planck Collaboration, 2020, A&A, 641, A6

Rasmussen C. E., 2003, Gaussian Processes in Machine Learning – In Summer School on Machine Learning, 63. Springer, Berlin, Heidelberg.

Renzi F., Silvestri A., 2020, preprint (arXiv:2011.10559)

Řípa J., Shafieloo A., 2019, MNRAS, 486, 3027

Ross N. P. et al., 2007, MNRAS, 381, 573

Sagredo B., Nesseris S., Sapone D., 2018, Phys. Rev. D, 98, 083543

Schneider P., 2006, Extragalactic Astronomy and Cosmology: An Introduction. Springer, Berlin

Scrimgeour M. I., 2012, MNRAS, 425, 116

Seikel M., Clarkson C., Smith M., 2012, J. Cosmol. Astropart. Phys., 06, 036

Shafieloo A., Kim A. G., Linder E. V., 2012, phys. Rev. D, 85, 123530

Silk J., 1968, ApJ, 151, 459

Song Y. S., Percival W. J., 2009, J. Cosmol. Astropart. Phys., 10, 004

Strauss M. A., Willick J. A., 1995, Phys. Rep., 261, 271

Sun W., Jiao K., Zhang T. J., 2021, preprint (arXiv:2105.12618)

Sunyaev R. A., Zeldovich Y. B., 1970, Ap&SS, 7, 3

Tarnopolski M., 2017, MNRAS, 472, 4819

Tegmark M. et al., 2006, Phys. Rev. D, 74, 123507

Velasquez-Toribio A. M., Fabris J. C., 2020, Eur. Phys. J. C., 80, 1

Zhang M. J., Li H., 2018, Eur. Phys. J. C, 78, 1

APPENDIX A: BARYON ACOUSTIC OSCILLATIONS INFLUENCE ON THE DPL APPROXIMATION

In Section 4.2, we have seen a discrepancy of 0.3 per cent between the fiducial model and the DPL model for $R_H \simeq 80$ Mpc h^{-1}. This small deviation in the fit can be attributed to the Baryon Acoustic Oscillations (BAO) signature, present around the scale 100 Mpc h^{-1}. To test this hypothesis, we perform our fit for the DPL approximation considering two estimates of the correlation function: one from the CLASS code and another for the case of absence of the BAO feature. For the last case, we use the fitting model given by Eisenstein & Hu (1998) and implemented in the code `nbodykit`[4] to obtain $\xi(r)$.

Fig. A1 shows the relative difference $\zeta_{DPL}/\zeta_{\Lambda CDM} - 1$ obtained calculating the correlation function with and without the BAO feature. It is evident the improvement in the fitting of ζ obtained
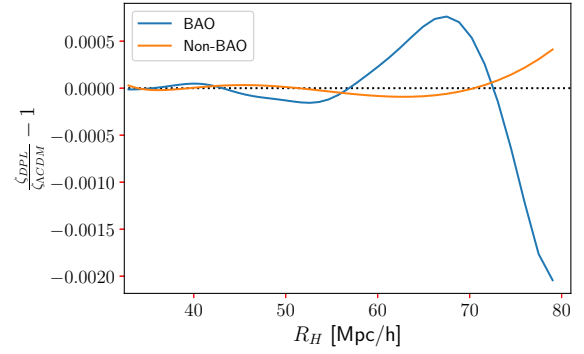
Figure A1. The relative difference $\zeta_{DPL}/\zeta_{\Lambda CDM} - 1$ obtained calculating the correlation function with and without the BAO feature.

from the correlation function without the BAO feature for $R_H < 40$ Mpc h^{-1}, with more significant effect for $R_H \gtrsim 55$ Mpc h^{-1} when compared to the correlation function with BAO.

APPENDIX B: STUDYING THE PARAMETER DEPENDENCE OF THE GROWTH RATE

In Section 3.1, we found a relation between $f(z)$ and $R_H(z)$ that is, in principle, explicitly independent of the ϵ parameter. However, when measuring $R_H(z)$, one needs to fix ϵ. Then, it is important to check if this criterion affects the $f(z)$ estimate. Here, we investigate the impact of fixing ϵ, as well as whether our choice of cosmological parameters might affect the $f(z)$ obtained.

We compare the result obtained from our fiducial model, $f^{\text{fiducial}}(z)$, using the input parameters

$$\left\{\epsilon, \ln\left(10^{10} A_s\right), \Omega_K, \Omega_c h^2\right\} = \{0.01, 3.045, 0.0, 0.1202\}, \quad (B1)$$

with the $f(z)$ resulting from the same fitting procedure but now varying these four parameters one at a time. The comparison is performed through the relative difference $f(z)/f^{\text{fiducial}}(z) - 1$.

Fig. B1 displays the relative difference between our input model and the 3 cases studied where $\epsilon = \{0.02, 0.05, 0.001\}$. These values correspond to different definitions of the homogeneity scale, R_H, where this scale is obtained when the data in analysis reaches 2 per cent, 0.5 per cent, and 0.1 per cent below the limit value 3, respectively (Scrimgeour et al. 2012). We show that for the redshift interval of interest, $0 < z < 2$, the error is below 0.5 per cent, which makes our approach robust with respect to ϵ. For the case $\epsilon = 0.001$, a divergent behaviour is observed around $z \sim 1.4$, where the function
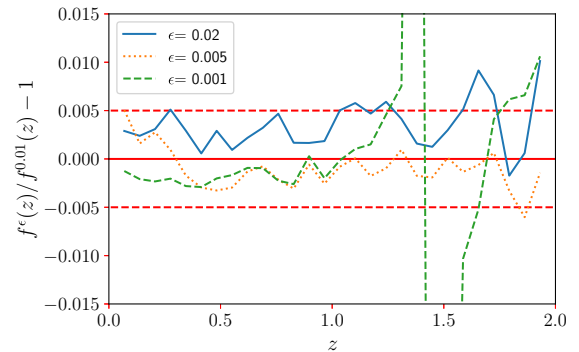
Figure B1. The relative difference for $f(z)$ between our fiducial model, i.e. $\epsilon = 0.01$, and the cases investigated with $\epsilon = \{0.02, 0.005, 0.001\}$.

---

[4] https://nbodykit.readthedocs.io/en/latest/
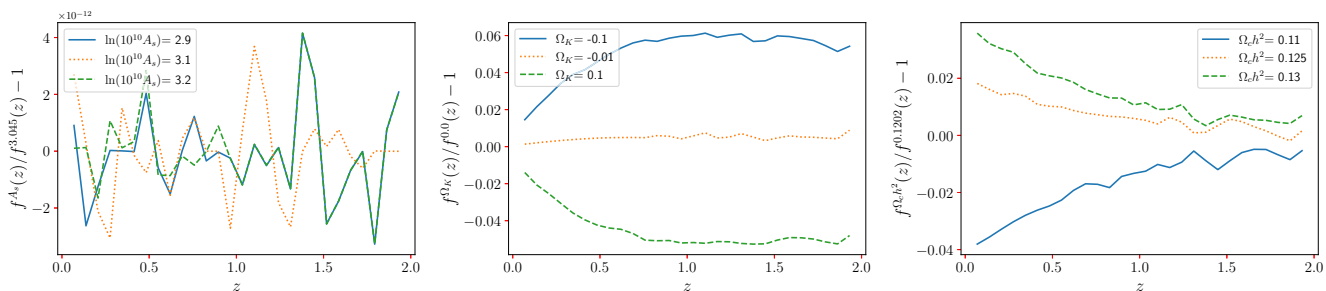
Figure B2. The relative difference, $f(z)/f^{\text{fiducial}}(z) - 1$, considering the variations, one at a time, of three cosmological parameters: $\ln(10^{10}A_s)$, Ω_K, and $\Omega_c h^2$. The left-hand panel shows the results for A_s, which is basically noise. The middle panel shows the outcomes for Ω_K where the relative difference is less than 6 per cent for the whole interval of interest. The right-hand panel shows the dependence on $\Omega_c h^2$ which is $\lesssim 4$ per cent, with the largest values for low z.

explodes up and come back from below. However, we notice that such small ϵ is unpractical when investigating R_H due to the statistical errors (and other systematics) inherent to the data analyses.

Fig. B2 shows $f(z)/f^{\text{fiducial}}(z) - 1$ for analyses obtained with the variation of three cosmological parameters one at a time: $\ln(10^{10}A_s)$, Ω_K, and $\Omega_c h^2$. For $\ln(10^{10}A_s)$ we use $\{2.9, 3.1, 3.2\}$, which is a large enough interval when we compare with the Planck best fit, namely, $\ln(10^{10}A_s) = 3.045 \pm 0.016$. Our results, displayed in the left-hand panel of Fig. B2, show nothing but statistical noise, indicating that our model is independent of $\ln(10^{10}A_s)$ values. For Ω_K, we consider $\{-0.1, -0.01, 0.1\}$ (see Fig. B2, middle panel). Also well beyond 2σ uncertainty for the Planck best fit $\Omega_K = -0.044 \pm 0.0165$. For all these cases, we observe a maximum of 6 per cent deviation, for the whole redshift interval. For all purposes, our approach has a small dependence on Ω_K considering a large interval of possible values.

For the analyses of the last parameter, $\Omega_c h^2$, we consider $\{0.11, 0.125, 0.13\}$. In these cases, we also find a slight dependence in our results, $\lesssim 4$ per cent, and decreasing for high z (see the right-hand panel of Fig. B2). As in the previous analyses, this result was somehow expected, because we are not modifying the meaning of $f(z)$, we just found an alternative way to find it. We already knew that the growth rate has a strong dependence in the matter density parameter, as seen in the parametrization $f(z) = \Omega_m(z)^\gamma$, where γ depends only on the constant of the equation of state, $\omega = -1$, for the ΛCDM case, or modifications according to the gravity model used.

APPENDIX C: CONSISTENCY TEST FOR DIFFERENT KERNELS

Our main result, i.e. the reconstruction of the homogeneity scale function, which, in turn, we use to derive the growth rate of structures, is based on the SE kernel. The SE kernel is a smooth covariance function that can reproduce global characteristics, although sometimes it cannot reproduce local characteristics.

As our data sample is nicely distributed, this kernel works smoothly. In order to test for possible systematic effects on the kernel choice, we examine our main results using this time the Matérn class kernels. The Matérn kernel can be written as

$$K_{M_\nu}(\tau) = \sigma_f^2 \frac{2^{1-\nu}}{\Gamma(\nu)} \left(\frac{\sqrt{2\nu}\,\tau}{l} \right)^\nu K_\nu \left(\frac{\sqrt{2\nu}\,\tau}{l} \right), \qquad (C1)$$

where K_ν is the modified Bessel function of second kind, $\Gamma(\nu)$ is the standard Gamma function and ν is a strictly positive parameter.
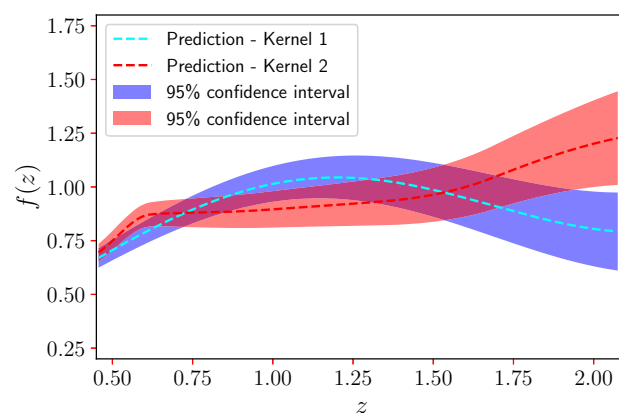
Figure C1. The reconstruction of the growth rate of structures $f^{R_H}(z)$ using two different kernels, namely, kernel 1 (the SE kernel) and kernel 2 (the Matérn kernel).

Here, the hyper-parameters σ_f and l are also optimized during the fitting.

Fig. C1 shows the best-fitting prediction and the GP reconstruction of the $f^{R_H}(z)$ function using the SE and the Matérn kernels. We do not find significant differences between both reconstructions; therefore, we conclude that they are statistically equivalent.

APPENDIX D: MEASUREMENTS OF THE GROWTH RATE FUNCTION

The literature reports diverse compilations of measurements of the growth rate of cosmic structures, $f(z)$ (see e.g. Basilakos 2012; Nunes et al. 2016; Sagredo et al. 2018), which we update here. Our compilation, shown in Table D1, follows three criteria in order to avoid or minimize possible data correlations, we consider: (i) $f(z)$ measurements obtained with cosmic tracers from different astronomical surveys or from disjoint redshift bins; (ii) direct measurements of f, and not measurements of $f\sigma_8$ that use a fiducial cosmological model to eliminate the σ_8-dependence; (iii) the latest measurement of f when the same astronomical survey performed two or more measurements corresponding to several data releases.

Table D1. Data compilation of $f(z)$ measurements that shares important features, as explained in the Appendix D.

Survey	z	f	Reference	Cosmological tracer
ALFALFA	0.013	0.56 ± 0.07	Avila et al. (2021)	H I extragalactic sources
2dFGRS	0.15	0.49 ± 0.14	Hawkins et al. (2003), Guzzo et al. (2008)	Galaxies
GAMA	0.18	0.49 ± 0.12	Blake et al. (2013)	Multiple-tracer: blue & red gals.
WiggleZ	0.22	0.60 ± 0.10	Blake et al. (2011)	galaxies
SDSS	0.35	0.70 ± 0.18	Tegmark et al. (2006)	Luminous red galaxies (LRG)
GAMA	0.38	0.66 ± 0.09	Blake et al. (2013)	Multiple-tracer: blue & red gals.
WiggleZ	0.41	0.70 ± 0.07	Blake et al. (2011)	Galaxies
2SLAQ	0.55	0.75 ± 0.18	Ross et al. (2007)	LRG & QSO
WiggleZ	0.60	0.73 ± 0.07	Blake et al. (2011)	Galaxies
VIMOS-VLT Deep Survey	0.77	0.91 ± 0.36	Guzzo et al. (2008)	Faint galaxies
2QZ & 2SLAQ	1.40	0.90 ± 0.24	Da Ângela et al. (2008)	QSO

This paper has been typeset from a TEX/LATEX file prepared by the author.